Journal of Materials Chemistry A

Dual-Responsive Jumping Actuators by Light and Humidity

Journal:	*Journal of Materials Chemistry A*
Manuscript ID	TA-ART-09-2022-007339.R1
Article Type:	Paper
Date Submitted by the Author:	11-Nov-2022
Complete List of Authors:	Li, Jingjing; Wuhan Textile University - Yangguang Campus; Nankai University Wang, Meilin; China Pharmaceutical University, Department of Science Cui, Zhanpeng; China Pharmaceutical University Liu, Shiyong; China Pharmaceutical University Feng, Danyang; Nankai University Mei, Guangkai; Nankai University Zhang, Rui; The University of Texas at Dallas, Department of Biochemistry & Biophysics An, Baigang; University of Science and Technology Liaoning, School of Chemical Engineering Qian, Dong; The University of Texas at Dallas, Department of Mechanical Engineering Zhou, Xiang; China Pharmaceutical University, Department of Science Liu, Zun-Feng; Nankai University, State Key Laboratory of Medicinal Chemical Biology, Key Laboratory of Functional Polymer Materials, Frontiers Science Center for New Organic Matter, College of Chemistry

Dual-Responsive Jumping Actuators by Light and Humidity

Jingjing Li[a,b]*, Meilin Wang[c], Zhanpeng Cui[c], Shiyong Liu[c], Danyang Feng[b], Guangkai Mei[b], Rui Zhang[d], Baigang An[e], Dong Qian[d], Xiang Zhou[c]*, Zunfeng Liu[b]*

[a]School of Textile Science and Engineering, Wuhan Textile University, Wuhan, Hubei, 430200, China

[b]State Key Laboratory of Medicinal Chemical Biology, Key Laboratory of Functional Polymer Materials, Frontiers Science Center for New Organic Matter, College of Chemistry, Nankai University, Tianjin 300071, China

[c]Department of Science, China Pharmaceutical University, Nanjing 211198, China

[d]Department of Mechanical Engineering, University of Texas at Dallas, Richardson, TX 75080, USA

[e]School of Chemical Engineering, University of Science and Technology Liaoning, Anshan 114051, China

Keywords: soft robotics, artificial muscle, jumping actuator, biomimetic, multiresponsive, photoresponse, moisture response, polymer composites, hydrogel

Abstract: Development of a multiresponsive miniaturized soft robot that can jump in different scenarios is highly desirable. This requires the actuator to simultaneously realize a large bending angle, a fast response, and a high actuation force under multiple stimuli to overcome its own weight. The difficulty lies in matching the material mechanical properties, response capacity, and interfacial adhesion of the different responsive layers. In this work, by mimicking the makeup application process, we

designed a synergistic actuator containing a photothermal expansion layer, an interfacial adhesion layer, and a moisture-responsive layer. Jumping actuation was achieved under near-infrared (NIR) light or moisture, where exceptionally high bending angle and bending speed were achieved when normalized to the thickness and temperature change. Inspired by frog jumping, direction-controlled jumping was realized by an asymmetric structural design. This work provides a new design strategy for miniaturized soft robots, sensors, and intelligent equipment.

1 Introduction

Inspired by biological behaviour in nature, various soft actuators that can achieve crawling, jumping, swimming, and other motions have aroused enormous interest.[1–9] Miniaturized soft jumping robots can cross barriers, perform search and rescue, and quickly escape from dangerous environments and therefore have attracted great attention. Until now, there have been only a few reports of soft jumping robots, achieved by employing light-triggered bimorph actuators, including graphene oxide (GO)/carbon nanotubes (CNTs),[10] carbon nitride polymers (CNPs),[11] CNTs/polydimethylsiloxane (PDMS),[12] CNTs/liquid crystal elastomers (LCEs),[13] and ladder polymer/CNTs.[14] However, to date, there have been no reports of actuators that can achieve jumping under multiple stimuli.

Light-driven actuation shows the advantage of remote control and delicate adjustment of the light source, but it is easily blocked by obstacles because of the linear propagation of light. Moisture can pass through obstacles via diffusion in pores to achieve actuation. Therefore, actuators that jump under multiple stimuli would

overcome the limitation of single-stimulus actuation and therefore work in different environmental scenarios. Here, the difficulty is that a combination of a fast-bending speed, a large bending curvature, and a high actuation force needs to be achieved under different stimuli.

Multi-stimuli bending deformation can be realized for a bimorph actuator by employing an active layer that responds to different stimuli[10,14] or employing a design in which different layers respond to different stimuli.[15–18] Materials responding to different stimuli exhibit rather different mechanical and interfacial properties, and therefore, how to achieve synergistic performance increments rather than mutual restriction of different layers is an important prerequisite for multiresponsive jumping. Currently, realizing good matching of several characteristics of different layers, including mechanical properties, multiresponsiveness, and interfacial adhesion, is still a challenge due to the rather limited material selection for multiresponsive actuators.

In this work, we realized a multiresponsive jumping actuator by consecutively applying an interfacial adhesion layer and a moisture-responsive porous layer on a photothermal expansion layer with inspiration from the makeup application process (Fig. 1a-c). During application of makeup on the face, different functional layers, such as a primer, cream foundations, a concealer, and other layers, are applied with fingers. Such a bottom-up fabrication process assembles multifunctional layers with good interfacial adhesion, uniformity, and well-controlled thickness. Under near infrared (NIR) light or sunlight, the photothermal expansion layer is heated and expands, and the moisture-responsive layer shrinks through water evaporation, causing a synergistic

bending actuation. By applying moisture, the moisture-responsive layer expands to realize bending actuation. Consequently, an exceptionally high bending actuation speed under NIR light or moisture is achieved (Fig. 1d and e). By further mimicking frog jumping, direction-controlled jumping actuation was achieved by an actuator design with anisotropic curvature.

2 Results and discussion

2.1 Preparation and characterization of the multiresponsive jumping actuator

Here, we describe the fabrication process of the jumping actuator. We first prepared a mixture solution of poly(vinylidene fluoride) (PVDF, 2.58 wt%) and carbon black (CB, 0.05 wt%) in *N*,*N*-dimethylformamide (DMF) by ultrasonication, which was poured into a stainless steel disk to form a 60-μm thin film by vapour evaporation at 60 °C. This PVDF-CB film was used as the photothermal expansion layer of the jumping actuator, on which the interfacial adhesion layer and the moisture layer were subsequently applied by smearing with a gloved finger. The adhesion layer was poly(2-ethylhexyl acrylate) (PEA) in ethyl acetate solution (45 wt%), which is a commercially available adhesive. The moisture-responsive layer was polyacrylamide (PAM) in water solution (7.9 wt%), which was prepared by radical polymerization of the acrylamide.[19] The introduction of the PEA layer can greatly increase the interfacial adhesion between the PVDF-CB and the PAM layers (Fig. S1, ESI†); otherwise, serious delamination was observed for the PAM/PVDF-CB bi-layer film (Fig. S2, ESI†). Uniform PEA and PAM layers can be obtained by such a finger-smearing process, and the thicknesses of these layers can be precisely adjusted by using different amounts of the precursor

solutions (Fig. S3, ESI†). This indicates that such a "makeup application"-like process is a suitable way to prepare multiple layers with uniform surfaces and well-controlled thicknesses. If not otherwise specified, the thicknesses of the PVDF-CB, PEA, and PAM layers were 60, 60, and 30 μm, respectively, for the following characterizations of physical properties and actuation performance. Such a smearing process is highly dependent on the viscosity and rheological properties of the gels. For example, we obtained a PAM hydrogel with increased viscosity and shear modulus by increasing the reaction time and monomer concentration (Fig. S4 and S5, ESI†). The results showed that the hydrogel with a viscosity of approximately 4000 Pa·s and a modulus of approximately 138.4 Pa can be easily smeared on the PVDF-CB substrate.

We next characterized the physical properties of the different functional layers. The PVDF-CB composite showed a rough surface (Fig. S6a, ESI†), which is preferred to increase its interfacial adhesion with the PEA layer. The N_2 absorption/desorption characterization indicated an average pore size of 144 nm for the PVDF-CB composite film, which would enable fast penetration of an organic vapour for actuation (Fig. S6b, ESI†). Fourier transform infrared (FTIR) spectra indicated nonpolar functional groups, such as -CH_2- (1167 cm^{-1}) and -CF_2- (1404 cm^{-1}), indicating strong interactions with hydrophobic molecules (Fig. S7a, ESI†).[20] The PVDF-CB layer showed strong light absorption from 200 to 2600 nm (Fig. S7b, ESI†), which spans the ultraviolet, visible, and IR light regions. When the PVDF-CB layer was irradiated by 200 mW cm^{-2} NIR light, the temperature quickly increased from 29 to 63 °C in 0.25 s, indicating a strong photothermal effect (Fig. S8, ESI†). The coefficient of thermal expansion (CTE) of the

PVDF-CB layer was as high as 400 × 10^{-6} K^{-1}, indicating its capacity for use as the photothermal expansion layer of the bimorph actuator.

The PEA showed polar and nonpolar groups, e.g., -C=O (1730 cm^{-1}), -C-O- (1238 cm^{-1}), C-O-C (1161 cm^{-1}), and -C-H (2858, 2926, 2960 cm^{-1}) (Fig. S9, ESI†),[21] which would allow the PEA to interact with both hydrophobic and hydrophilic polymers and serve as an interfacial adhesive layer. The FTIR spectrum of the PAM hydrogel shows N-H stretching (3188, 3338 cm^{-1}), N-H bending (1650 cm^{-1}), and C-O stretching (1600 cm^{-1}) peaks.[22] Fig. S10 shows a large difference of water contact angle between the PAM side (45.39 °) and the PVDF-CB side (86.90 °), indicating a difference in hydrophilicity. A 10-μm-thick PAM film was obtained by applying the PAM gel on the PVDF-CB substrate, followed by drying and peeling off. The PAM film contained 29% water at an environmental relative humidity (RH) of 40%, and its length, width, and thickness increased with increasing environmental humidity. Fig. S11 shows that with RH increased from 40% to 90%, the thickness, width, and length of the PAM layer increased by 36.8%, 11.9%, and 16.6%, corresponding to a large size change of 6.73%, 4.93%, and 2.82% per 10% change of RH, respectively. Such a large volume expansion is highly important to realize a large bending angle of the actuator under moisture stimuli. Thermogravimetric analysis (TGA) of the PAM film showed a water loss of 6.5% as the temperature increased from 37 to 100 °C (Fig. S12, ESI†), and heating the PAM film in an oven from 30 to 80 °C resulted in a thickness decrease of 35%. It exhibited a negative CTE of –390 × 10^{-6} K^{-1}, obtained by a dilatometer. Fig. 1c shows a highly porous structure of the PAM layer, which is rather important for fast mass

transport of water molecules, to allow fast absorption and desorption of water moisture during actuation and de-actuation. The PAM exbibits a specific surface area of 1.05 m^2 g^{-1}, a specific pore volume of 0.0022 cm^3 g^{-1}, and an average pore size of 82.6 nm (Fig. S13, ESI†). In addition, to investigate the morphology change of the PAM layer before and after moisture absorption, we took the optical microscope images of the PAM layer before and after moisture absorption (Fig. S14, ESI†). The photos indicated that the texture expands after water moisture absorption. These characteristics would highly facilitate rapid absorption and desorption of water molecules from the PAM layer, which can be used as the moisture-responsive layer of the actuators.

The photothermal water desorption and absorption kinetics of the PAM layer and the PVDF-CB/PEA/PAM were then investigated. Under irradiation with 250 mW cm^{-2} NIR light, the 20-μm thick PAM layer lost 29.27% mass in approximately 9.8 min, and it could hardly recover the initial mass after switching off the NIR light; in comparison, the PVDF-CB/PEA/PAM actuator lost ~20.5% of the PAM mass in 7 min, which could be completely recovered after switching off the NIR light (Fig. S15, ESI†). The decreased water loss of the PVDF-CB/PEA/PAM compared to the PAM film under NIR irradiation and the increased water reabsorption after switching off the NIR light can be ascribed to the fact that the PEA layer serves as a water supply for the PAM layer because of the good interfacial interaction between these layers.

We then characterized the mechanical properties of the PAM, PVDF-CB, PVDF-CB/PEA, and the PVDF-CB/PEA/PAM films, which exhibited breaking strengths of 38, 16, 11, and 16 MPa, and the breaking strains of 3.9%, 68%, 45%, and 47%,

respectively (Fig. S16, ESI†). The highly increased breaking strain of the PVDF-CB/PEA/PAM compared to that of the PAM should be attributed to the introduction of the PEA adhesive layer, which showed efficient load transfer from the PVDF-CB layer to the PAM layer. The PAM layer exhibits a modulus of 2452 MPa, which is rather high compared to the common PAM hydrogel (<0.1 MPa).[19] This is a key factor to allow the jumping actuator to generate a high actuation stress. The PVDF-CB/PEA/PAM film could be used as an effective jumping actuator driven by light and moisture, benefiting from the following properties: including a high modulus of PAM to achieve high actuation stress, a high-volume expansion and photothermal effect of the PVDF-CB layer under light, a high-volume expansion of PAM to realize a large bending curvature under moisture, a large difference in hydrophilicity between PAM and PVDF-CB layer, and the porous structure of PAM film to allow fast absorption and desorption of water molecules under light irradiation.

2.2 Photothermal jumping actuation of the PVDF-CB/PEA/PAM actuator

Here, we investigated the photothermal reversible bending actuation of the PVDF-CB/PEA/PAM actuator under light irradiation (NIR and sunlight) (Fig. 2a). We optimized the actuation performances by varying the thickness of PAM layer (15, 30, 45, and 60 μm) and keeping the PVDF-CB layer constant at 60 μm (Fig. S17, ESI†). The maximum bending angle was obtained at a thickness of the PAM layer of 30 μm, corresponding to a thickness ratio of 2 of the PVDF-CB to PAM layer. The following research of the actuator will be carried out at this ratio of 2. A flat PVDF-CB/PEA/PAM film (15 mm × 2 mm × 150 μm) bent 199° to the PAM side in 0.6 s under irradiation

with 250 mW cm^{-2} NIR light at an environmental RH of 35%, corresponding to a bending curvature of 2.3 cm^{-1}. The actuator film almost returned to its original position after one cycle of actuation under NIR irradiation (Fig. S18, ESI†). When the light continuously irradiated on the actuator film, the actuator quickly approached to the maximum bending angle and fluctuated slightly to keep oscillating, possibly due to the rapid absorption and desorption of water molecules of the PAM layer (Fig. S19, ESI†). The energy conversion efficiency was calculated to be 5.29% (Note S1, ESI†), according to the reported literature.[28] This energy conversion efficiency is among the best of the reported actuators (e.g., 0.01% for PC/CNT actuator,[28] 0.02% for PE/*I*-MXene,[24] and 0.0019% for PE/CNT[27]). During this actuation process, the temperature increased from 28.5 to 63.2 °C, corresponding to a temperature change of 34.7 °C; the actuator recovered to the initial state after switching off the NIR light by water reabsorption. Such a fast actuation at a small temperature increment is a result of the synergistic effect of photothermal volume expansion of the PVDF-CB layer and volume shrinkage of the PAM layer due to water loss, which was stable for the investigated 1000 actuation cycles (Fig. 2b). The actuation bending angle of the PVDF-CB/PEA/PAM actuator under 250 mW cm^{-2} NIR light in a closed space is slightly smaller than that in an open space, with the maximum bending angle of 199° for the closed space and 159° for the open air (Fig. S20, ESI†). Increasing the environmental RH resulted in a decreased actuation bending angle and decreased actuation bending speed (Fig. S21a, ESI†). Increasing the environmental temperature resulted in an increased actuation bending angle and increased actuation bending speed (Fig. S21b,

ESI†). The actuation performance can be further improved by decreasing the film thickness or increasing the light intensity. Decreasing the film thickness of the PVDF-CB/PEA/PAM actuator from 150 to 20 μm resulted in an increased bending angle from 199 to 382°, with the actuation temperature negligibly changing (Fig. S22, ESI†). This should be a result of the combination of decreased film rigidity and increased heat transfer through the thickness direction of the actuator with decreasing film thickness. Increasing the NIR light intensity from 110 to 250 mW cm^{-2} resulted in an increase in the bending angle from 109 to 199°, a decrease in the response time from 0.60 to 0.56 s, and an increase in the actuation speed from 3.8 to 7.9 cm^{-1} s^{-1}, accompanied by an increase in the temperature change from 15 to 34.7 °C (Fig. 2c). To better investigate the actuation mechanism, a theoretical analysis of the PVDF-CB/PEA/PAM actuator was conducted[17]. We first employed a transient heat transfer analysis to quantify the temperature change of the actuator as a function of irradiation time at a light intensity of 68 mW cm^{-2}, and the obtained theoretical values were consistent with the experimental measurement for the actuator (Fig. S23 and Note S2, ESI†). Then, a thermomechanical analysis was conducted to simulate the bending angle as a function of the temperature change by employing the classical Timoshenko beam theory (Note S3, ESI†). The calculated values of the temperature change and bending angle at different light intensities agree well with the experimental observations, which are almost linearly proportional to the light intensity (Fig. 2c). Interestingly, fast actuation was achieved for the PVDF-CB/PEA/PAM actuator under exposure to sunlight. A PVDF-CB/PEA/PAM actuator (20 mm × 2 mm × 20 μm) bent 132°, reaching a bending

curvature of 1.2 cm^{-1}, in 0.57 s under exposure to sunlight, with a temperature increment from 28.5 to 34.6 °C (Fig. S24, ESI†). By shading it from sunlight, the actuator recovered the initial shape. The sunlight responsiveness of the PVDF-CB/PEA/PAM actuator provides a possibility for applications in soft robots directly driven by solar energy, in solar energy harvesting and in sensing.

The actuation stress under photothermal actuation was then investigated. A PVDF-CB/PEA/PAM film (20 mm × 2mm × 150 μm) was loaded with a 1.75 MPa stress on a mechanical tester. By switching on 250 mW cm^{-2} NIR light, the stress decreased to 0.8 MPa in 8 s, corresponding to an actuation stress of 0.95 MPa. The loading stress returned to 1.75 MPa with switching off the NIR light. Increasing the light intensity from 110 to 250 mW cm^{-2} resulted in a monotonic increase in the actuation stress from 0.14 to 0.95 MPa (Fig. S25, ESI†). Because the actuation performance is highly related to the film dimensions, the response speed or bending curvature was multiplied by the film thickness and divided by the temperature change to obtain the normalized response speed (16.57×10^{-4} s^{-1} $°C^{-1}$) or normalized bending curvature (9.94×10^{-4} $°C^{-1}$), respectively. Because a larger thickness resulted in a slower thermal transfer, the response time was divided by the film thickness to obtain a normalized value (0.004 s μm^{-1}) (Fig. 2d).

The normalized bending curvature (8.46×10^{-4} $°C^{-1}$) for such a small temperature increment (10.5 °C) is among the best for the photothermal bimorph actuators reported thus far (Fig. 2e, and Table S1, ESI†),[12,17,18,23–29] e.g., biaxially oriented polypropylene (BOPP)/graphite/paper actuators (3.07×10^{-4} $°C^{-1}$ for a ΔT of 41.4 °C),[18]

MXene/polyethylene (PE) actuators (5.79×10^{-4} °C^{-1} for a ΔT of 29 °C)[24], PE/CNT actuators (6.94×10^{-4} °C^{-1} for a ΔT of 28.8 °C),[27] and polyimide (PI)/paraffin wax/CNT actuators (1.22×10^{-4} °C^{-1} for a ΔT of 20 °C).[29] The normalized actuation speed (15.10×10^{-4} s^{-1} °C^{-1}) for such a short response time (0.56 s) is also among the best for photothermal bimorph actuators reported thus far (Fig. 2f), e.g., ink/polyethylene terephthalate (PET)/acrylic actuators (10.67×10^{-4} s^{-1} °C^{-1} for a response time of 0.36 s),[17] PE/CNT actuators (4.96×10^{-4} s^{-1} °C^{-1} for a response time of 1.4 s),[27] PDMS/CNT actuators (4.73×10^{-4} s^{-1} °C^{-1} for a response time of 0.83 s),[12] and MXene/PE actuators (2.76×10^{-4} s^{-1} °C^{-1} for a response time of 2.1 s).[24] The large bending curvature, fast response speed, and high actuation stress encouraged us to investigate the possibility of photothermal jumping actuation of the PVDF-CB/PEA/PAM actuator.

Here, we achieved photothermal jumping actuation of the PVDF-CB/PEA/PAM actuator by mimicking the frog jumping. A frog sitting back on its feet extends its legs to push off of the ground and explosively jump (Fig. 1b). During such a process, the frog jumps up and forward by anisotropically extending the hind legs more than the forelegs. The PVDF-CB/PEA/PAM actuator (20 mm × 1.5 mm × 20 μm) was shaped into an arc architecture with the PAM layer on the inner side, which was placed on a zigzag surface with the two legs touching the ground. In Fig. 3a and b, the leg touching the vertical surface served as the hind leg and realized a directional jump (forward or backward) (Fig. S26 and Movie S1, ESI†). Upon irradiation by 200 mW cm^{-2} NIR light for 1.08 s, the actuator suddenly jumped 4.5 mm high by pushing the hind leg into the ground and decreasing the bending curvature. At the same time, the actuator jumped

forward by 37.5 mm (Fig. S27, ESI†). An initial jumping speed of 5.6 cm s^{-1} and a specific work capacity of 0.16 J kg^{-1} were achieved for this jumping process, and no performance decay occurred during multiple jumping times. The normalized jumping height (2.81 mm mg^{-1}), initial jumping speed (5.6 cm s^{-1}), and specific work capacity (0.16 J kg^{-1}) are at the same level as those of the photothermal jumping actuators reported thus far (Table S2, ESI†).[10–14,30] Under light irradiation, the work capacity for the actuator with a thickness of 20 μm was 0.16 J/kg, and then decreased to 0 J/kg as this thickness further increased greater than 20 μm.

Such direction-controlled jumping was also realized on a flat rough surface. Here a PVDF-CB/PEA/PAM film (10 mm × 1.5 mm × 20 μm) was shaped into an anisotropic curved architecture with the PAM layer on the inner side, employing the leg with a larger bending curvature as the hind leg. Upon irradiation by 250 mW cm^{-2} NIR light, the bending curvature of the arc-shaped actuator increased such that the "hind leg" of the jumping actuator extended to jump up and forward (Fig. 3c, Fig. S28, and Movie S2, ESI†). Such a direction-controlled jumping actuation would provide the miniaturized robot with the capacity to reach a targeted location by crossing the barriers via remotely controlled light stimulation.

2.3 Moisture-driven bending and jumping actuation

In this section, we characterized the bending actuation of the PVDF-CB/PEA/PAM actuator driven by moisture. A PVDF-CB/PEA/PAM film (15 mm × 2 mm × 150 μm) showed reversible bending actuation when applying/removing moisture (Fig. 4a). Such moisture-driven actuation showed high repetitiveness, and no

performance decay was observed for the investigated 1000 bending-unbending actuation cycles (Fig. 4b). Actuation by applying a flux of moisture (8 mg s^{-1}) highly increased the actuation speed. A bending speed of 4125° s^{-1} was obtained, for a response time of 0.04 s, which is among the best for moisture-driven actuators thus far (Fig. 4c). The bending angle of the bimorph actuators is highly affected by the dimensional parameters, e.g., the film thickness and length. For example, decreasing the actuator thickness resulted in an increase in the bending angle and a decrease in the response time (Fig. S29, ESI†). Therefore, we multiplied the response speed or bending angle by the film thickness to obtain the normalized response speed (82500° μm s^{-1}) or normalized bending angle (43800° μm), respectively, which are also among the best compared to those reported for bimorph actuators thus far,[31–41] such as the GO-CNT actuator (3500° μm s^{-1}, 280° μm),[10] the cross-linked liquid crystal polymer (CLCPs) actuator (6300° μm s^{-1}, 2520° μm),[33] the $CaCO_3$ oligomer/PVDF actuator (17430° μm s^{-1}, 5229° μm),[38] and the sodium alginate (SA)/PVDF actuator (550° μm s^{-1}, 7700° μm)[41] (Fig. 4d and Table S3, ESI†).

The actuation force during moisture-driven actuation of the PVDF-CB/PEA/PAM actuator was then investigated. A PVDF-CB/PEA/PAM film (20 mm × 2 mm × 20 μm) was loaded with a 5.0 MPa stress on a mechanical tester, and the stress was decreased to approximately 4.0 MPa in over 1.0 s by applying a flux of moisture (15 mg s^{-1}), corresponding to a 1.0 MPa stress generation (Fig. S30a, ESI†). As the film thickness increased from 20 to 150 μm, the actuation stress decreased from 1.0 to 0.34 MPa (Fig. S30b, ESI†). This should be ascribed to the fact too-thick PEA and PAM layers

decrease the modulus of the film and therefore decrease the generated actuation stress. The above results of the combination of high actuation speed and high actuation stress in a short response time encouraged us to investigate the possibility of achieving moisture-driven jumping actuation of the PVDF-CB/PEA/PAM actuator.

Here, a PVDF-CB/PEA/PAM film (20 mm × 1.5 mm × 20 μm) was shaped into a curved architecture (like the number "6") with the PAM layer on the inner side, which was placed on the ground with the PVDF-CB side touching the ground. Upon application of sonication-generated moisture, for the first 3.48 s, both ends (the free "A" end and the restricted "B" end) slightly unbent such that the "D" part touched the ground. Suddenly, in the following 0.08 s, the "B" end explosively actuated and unbent upward, and the "D" part pushed into the ground, throwing the PVDF-CB/PEA/PAM actuator into the air and causing it to jump by 13.2 mm. The initial velocity reached 0. 17 m/s, thereby generating a specific work capacity of 0.01 J/kg (Fig. 5a-c, and Movie S3, ESI†).

Such jumping actuation is highly affected by the film thickness. The jumping height decreased with increasing film thickness (Fig. 5d). The work capacity for the actuator increased from 0.005 to a maximum value of 0.01 J/kg as the thickness of PVDF-CB/PEA/PAM decreased from 45 to 20 μm, and then decreased to 0 J/kg as this thickness further increased to >90 μm (Fig. S31, ESI†). To the best of our knowledge, this is thus far the first jumping actuator driven by moisture, which would provide wide application possibilities because of the high accessibility of moisture in air. The jumping height (13.2 mm) is comparable to that of jumping actuators driven by other

stimuli, such as light-driven actuators (0.84 mm for GO-CNTs,[10] 10 mm for CNPs,[11] 32 mm for CNTs/PDMS[12]) and organic vapour-driven ladder polymer/CNTs (26 mm).[14]

2.4 Multimorphing, multimotions, gripping, walking, and self-oscillation of the PVDF-CB/PEA/PAM actuator

Animals can perform different types of locomotion and actions for survival. Here we show that in addition to jumping, the PVDF-CB/PEA/PAM actuator can perform multimorphing, multi-motions, grasping, walking, and self-oscillation (Movie S4, ESI†). The PVDF-CB/PEA/PAM film can be shaped into different architectures by thermal setting at 60 °C for 1 h. If not otherwise specified, the PAM is on the inner side of the curves for the following examples, and the actuator exhibits moisture-driven bending actuation towards the PAM side. Multimorphing was realized, including actuation of an "8"-shaped film into a letter "S" shape, straightening of a "heart"-shaped actuator and a spiral actuator, and "flower" blooming (Fig. S32, ESI†). In addition, rolling, folding, and turning over were also achieved for a spiral PVDF-CB/PEA/PAM actuator stimulated by a flux of moisture. Under illumination by NIR light, an arc-shaped PVDF-CB/PEA/PAM actuator can close its arms and serve as a clamp to capture 78 times its own weight (Fig. S33, ESI†). Bending actuation was also observed for the PVDF-CB/PEA/PAM film in response to organic vapour, e.g., ethyl acetate, acetone, dichloromethane, ethanol, petroleum, and methanol, which bent to the PAM side as the organic vapour was absorbed in the PVDF-CB layer (Fig. S34, Tables S4 and S5, ESI†).[42–46] An asymmetric arc-shaped PVDF-CB/PEA/PAM actuator with the PAM as the inside layer was demonstrated to locomote forward in response to ethanol vapour

(Fig. S35, ESI†).

Interestingly, a straight PVDF-CB/PEA/PAM film (20 mm × 2 mm × 20 μm) showed self-oscillatory actuation with environmental humidity and temperature fluctuations (Fig. S36, ESI†), and an arc-shaped PVDF-CB/PEA/PAM film with the PAM on the outer side placed on a flat surface showed self-oscillatory swinging together with slight oscillation of the curvature (Fig. S37, ESI†). Such a slightly curved PVDF-CB/PEA/PAM film fully curved into a circle when it was vertically placed 1−2 mm above a palm and did not show oscillation (Fig. S38, ESI†). Increasing the distance above the palm to 5 mm recovered the self-oscillatory actuation of the PVDF-CB/PEA/PAM film (Fig. S39a, ESI†), which showed a much larger oscillation amplitude compared to that when it was not above a palm. This indicates that the fluctuation of the environmental humidity and temperature highly affect the self-oscillation. In addition, decreasing the thickness of the PVDF-CB/PEA/PAM actuator also increased the bending amplitude during self-oscillation (Fig. S39b, ESI†). This self-oscillating behaviour would provide the PVDF-CB/PEA/PAM actuator with applicability in self-sustained soft robots, sensors, and smart equipment.

3 Conclusion

In summary, a multiresponsive jumping actuator was prepared by mimicking the "makeup application" process. Jumping can be triggered by light or moisture, which originates from the indispensable synergistic combination of the photothermal layer and moisture-responsive layer bonded by the adhesion layer. In response to NIR light, the actuator exhibited a high actuation stress of 0.95 MPa, a large bending angle of 9.94 ×

10^{-4} (°C)$^{-1}$, a high bending speed of 16.57 × 10^{-4} (s °C)$^{-1}$, and a short response time of 0.56 s; in response to moisture, the actuator exhibited a large bending angle of 43800° μm and a high bending speed of 82500° μm s^{-1}. Jumping was realized in response to both NIR light and moisture. Multistimuli jumping actuation can overcome the restriction of actuation driven by a single stimulus and therefore provides additional possibilities to work in more complex environmental conditions. Such a multilayer design of jumping actuators could inspire new design strategies for multifunctional compact robots and smart equipment. Additionally, the actuator also exhibited self-sustained oscillation, multimorphing, grasping, and walking under organic vapours. This special design could provide new opportunities for miniaturized robots for use in multiple terrains or in biomedical and surgical operations, sensors, and other biomimetic applications.

4 Experimental method

4.1 Preparation of PVDF-CB film, PAM

The PVDF (0.25, 0.175, 0.125, 0.0625, and 0.0313 g) and CB (0.005, 0.0075, 0.0025, 0.0012, and 0.0006 g) were mixed in DMF (10, 10, 8 , 6, and 4 mL) for 30 min by mechancial stirring at 40 °C, then different amount of mixture was poured into a mould and let stand for 5 h at 40 °C to evaporate the DMF to obtain the PVDF-CB film with different thicknesses.

The PAM hydrogel was prepared by free radical polymerization of acrylamide. Briefly, vinyl-triethoxysilane (3.8 g) was completely dissolved into deionized water (30 mL) to form a transparent dispersion to prepare vinyl functionalized silica nanoparticles

for using as cross-linking reagent. The diluted dispersion (0.1 wt%, 9.5 mL) was added into acrylamide (0.7000 g) and ammonium persulfate (0.0035 g) and stirred for 0.5 h. Then the solution was degassed and sealed under N_2 and reacted at 42 °C for 12 h to obtain the PAM hydrogel. For the following measurements of viscosity and rheology, different feed ratio and reaction time are used.

4.2 Preparation of PVDF-CB/PEA/PAM actuator

The PEA (1 mL, Yida Co. Ltd.) was applied on a PVDF film (4 cm × 2 cm) by smearing with a gloved finger and annealed in an oven (100 °C) for 20 min, followed by applying PAM (0.5 mL) and air-dried for 10 min to obtain a PVDF-CB/PEA/PAM, where the thickness of PEA and PAM were 60 and 30 μm, respectively. Different thickness of the PEA and PAM layers were obtained by changing the amount of the PEA solution and PAM gel, and the PVDF-CB/PEA/PAM films with different thicknesses (20 to 150 μm) were obtained, with the thickness ratio of PVDF-CB/PEA/PAM at 2/2/1. The PVDF-CB/PEA/PAM actuators with different dimensions and shapes were obtained by shaping the PVDF-CB/PEA/PAM film into the required architecture and annealed at 60 °C for 2 h to thermal set the shape.

4.3 Characterizations

The scanning electron microscope (JEOL, JSM-6701F, Japan) were used to obtain the morphology and the film thickness. The absorption spectrum was obtained by UV/vis/IR spectrometer (Shimadzu, UV3600 plus, Japan). FTIR spectroscopy was performed on each layer of the actuator using a spectrometer (Nicolet IS50, USA). The TGA analysis was performed using a thermal analyzer (Netzsch, STA449F3, Germany).

The coefficient of thermal expansion was measured on a dilatometer (Netzsch, DIL 402SE, Germany). The contact angle was measured using a contact angle-measuring instrument (Powereach, JC2000D1, China). The mechanical properties were obtained by an Instron mechanical tester (Model 3365, China). The surface area and porosity were obtained on a surface area analyzer (Gemini 2390, USA). The viscosity was obtained on a rheometer (Anton Paar GmbH MCR702, Germany). An IR camera was used to obtain the actuation temperature (FLIR T440, American). The bending amplitude and response time of the actuators were obtained from digital images captured by a video camera (SONY, HDR-PJ600E, Japan). The light intensity was obtained on an IR power meter (Lianhuicheng, LH-129, China), and the RH was measured using a hygrometer (Jianda Renke Co., Ltd., LM12-COS-03-5, China).

Author contributions

Z. Liu, X. Zhou, and J. Li conceived the project. All authors contributed to the experiments, data analysis, and writing.

Conflicts of interest

There are no conflicts to declare.

Acknowledgement

This work was supported by the National Key Research and Development Program of China (grant SQ2019YFE012189), the National Natural Science Foundation of China (grants 51973093, U1533122, and 51773094), “Frontiers Science Center for New Organic Matter”, Nankai University (Grant Number 63181206), National Special

Support Plan for High-level Talents people (grant number C041800902), the Science Foundation for Distinguished Young Scholars of Tianjin (grant number 18JCJQJC46600), State Key Laboratory for Modification of Chemical Fibers and Polymer Materials, Donghua University (grant LK1704), Xingliao Talent Plan (grant number XLYC1802042), the Key Research Projects, the grant from the US National Science Foundation (Award CMMI-1727960) and Eugene McDermott Graduate Fellowship at the University of Texas at Dallas.

References

1 X. L. Zhu, Y. Hu, G. Wu, W. Chen and N. Z. Bao, *ACS Nano,* 2021 **15**, 9273−9298.

2 P. D. Li, N. Su, Z. Y. Wang and J. S. Qiu, *ACS Nano,* 2021, **15**, 16811−16818.

3 Z. W. Li, N. V. Myung and Y. D. Yin, *Sci. Robot.,* 2021, **6**, eabi4523.

4 Q. Zhao, J. W. C. Dunlop, X. L. Qiu, F. H. Huang, Z. B. Zhang, J. Heyda, J. Dzubiella, M. Antonietti and J. Y. Yuan, *Nat. Commun*., 2014, **5**, 4293.

5 D. Melling, J. G. Martinez and E. W. H. Jager, *Adv. Mater*., 2019, **31**, 1808210.

6 J. Gong, E. Hosaka, K. Sakai, H. Ito and Y. Shibata, *Polymer*, 2018, **10**, 486.

7 Z. C. Zhu, K. Asaka, L. F. Chang, K. Takagi and H. L. Chen, *J. Appl. Phys.,* 2013, **114**, 084902.

8 G. M. Spinks, N. D. Martino, S. Naficy, D. J. Shepherd and J. Foroughi, *Sci. Robot.,* 2021, **6**, eabf478.

9 P. Won, K. K. Kim, H. Kim, J. J. Park, I. Ha, J. Shin, J. Jung, H. Cho, J. Kwon, H. Lee and S. H. Ko, *Adv. Mater*., 2021, **33**, 2002397.

10 H. Li and J. F. Wang, *ACS Appl. Mater. Interfaces,* 2019, **11**, 10218−10225.

11 H. Arazoe, D. Miyajima, K. Akaike, F. Araoka, E. Sato, T. Hikima, M. Kawamoto and T. Aida, *Nat. Mater.,* 2019, **15**, 1084–1089.

12 Y. Hu, J. Q. Liu, L. F. Chang, L. L. Yang, A. F. Xu, K. Qi, P. Lu, G. Wu, W. Chen and Y. C. Wu, *Adv. Funct. Mater*., 2017, **27**, 1704388.

13 C. Ahn, X. D. Liang and S. Q. Cai, *Adv. Mater. Technol*., 2019, **4**, 1900185.

14 K. Q. Yu, X. Z. Ji, T. Y. Yuan,Y. Cheng, J. J. Li, X. Y. Hu, Z. F. Liu, X. Zhou and L. Fang, *Adv. Mater.,* 2021, **33**, 2104558.

15 P. D. Zhou, L. Z. Chen, L. Q. Yao, M. C. Weng and W. Zhang, *Nanoscale,* 2018, **10**, 8422.

16 J. J. Li, L. L.Mou, R. Zhang, J. K. Sun, R. Wang, B. G. An, H. Chen, K. Inoue, R. Ovalle-Robles and Z. F. Liu, *Carbon,* 2019, **148**, 487–495.

17 J. J. Li, R. Zhang, L. L. Mou, M. Jung de Andrade, X. Y. Hu, K. Q. Yu, J. K. Sun, T. J. Jia, Y. Y. Dou, H. Chen, S. L. Fang, D. Qian and Z. F. Liu, *Adv. Funct. Mater.,* 2019, **29**, 1808995.

18 M. C. Weng, P. D. Zhou, L. Z. Chen, L. L. Zhang, W. Zhang, Z. G. Huang, C. H. Liu and S. S. Fan, *Adv. Funct. Mater.,* 2016, **26**, 7244–7253.

19 Y. Huang, M. Zhong, F. K. Shi, X. Y. Liu, Z. J. Tang, Y. K. Wang, Y. Huang, H. Q. Hou, X. M. Xie and C. Y. Zhi, *Angew. Chem. Int. Ed.*, 2017, **56**, 9141–9145.

20 B. P. S. Santos, J. J. R. Arias, F. E. Jorge, R. É. P. D. Santos, B. S. Fernandes, L. S. Candido, A. C. C. Peres, É. G. Chaves and M. F. V. Marques, *Mater. Today Commun*., 2021, **26**, 101743.

21 S. Bajpai, J. S. P. Rai and I. Nigam, *J. Appl. Polym. Sci.,* 2011, **122**, 676–684.

22 W. Q. Kong, C. W. Wang, C. Jia, Y. D. Kuang, G. Pastel, C. J. Chen, G. G. Chen,

S. M. He, H. Huang, J. H. Zhang, S. Wang and L. B. Hu, *Adv. Mater.,* 2018, **30**, 1801934.

23 J. Yang, J. X. Zhang, X. L. Li, J. W. Zhou, Y. P. Li, Z. P. Wang, J. L. Cheng, Q. Guan and B. Wang, *Nano Energy,* 2018, **53**, 916–925.

24 Y. Hu, L. L. Yang, Q. Y. Yan, Q. X. Ji, L. F. Chang, C. C. Zhang, J. Yan, R. R. Wang, L. Zhang, G. Wu, J. Sun, B. Zi, W. Chen and Y. C. Wu, *ACS Nano,* 2021, **15**, 5294–5306.

25 G. F. Cai, J. H. Ciou, Y. Z. Liu, Y. Jiang and P. S. Lee, *Sci. Adv*., 2019, **5**, eaaw7956.

26 J. K. Mu, C. Y. Hou, H. Z. Wang, Y. Li, Q. H. Zhang and M. F. Zhu, *Sci. Adv*., 2015, **1**, e1500533.

27 L. P. Li, J. X. Meng, C. Y. Hou, Q. H. Zhang, Y. G. Li, H. Yu and H. Z. Wang, *ACS Appl. Mater. Interface,* 2018, **10**, 15122–15128.

28 X. B. Zhang, Z. B. Yu, C. Wang, D. Zarrouk, J. W. T. Seo, J. C. Cheng, A. D. Buchan, K. Takei, Y. Zhao, J. W. Ager, J. J. Zhang, M. Hettick, M. C. Hersam, A. P. Pisano and R. S. Fearing, *Nat. Commun*., 2014, **5**, 2983.

29 J. Deng, J. F. Li, P. N. Chen, X. Fang, X. M. Sun, Y. S. Jiang, W. Weng, B. J. Wang and H. S. Peng, *J. Am. Chem. Soc*., 2016, **138**, 225.

30 J. Jeon, J. C. Choic, H. Lee, W. Cho, K. Lee, J. G. Kim, J. W. Lee, K. I. Joo, M. Cho, H. R. Kim and J. J. Wie, *Mater. Today,* 2021, **49**, 97–106.

31 R. C. Lan, Y. Z. Gao, C. Shen, R. Huang, J. Y. Bao, Z. P. Zhang, Q. Wang, L. Y. Zhang and H. Yang, *Adv. Funct. Mater.,* 2021, **31**, 2010578.

32 D. D. Han, Y. L. Zhang, H. B. Jiang, H. Xia, J. Feng, Q. D. Chen, H. L. Xu and H.

B. Sun, *Adv. Mater*., 2015, **27**, 332–338.

33 Y. Y. Liu, B. Xu, S. T. Sun, J. Wei, L. M. Wu and Y. L.Yu, *Adv. Mater.,* 2017, **29**, 1604792.

34 Y. Q. Zhang, H. Y. Jiang, F. B. Li, Y. H. Xia, Y. Lei, X. H. Jin, G. Z. Zhang and H. J. Li, *J. Mater. Chem. A,* 2017, **5**, 14604–14610.

35 G. C. Xu, J. Chen, M. Zhang and G. Q. Shi, *Sensor. Actuat. B: Chem*., 2017, **242**, 418–422.

36 Y. H. Ge, R. Cao, S. J. Ye, Z. Chen, Z. F. Zhu, Y. F. Tu, D. T. Ge and X. M. Yang, *Chem. Commun.,* 2018, **54**, 3126–3129.

37 J. Cao, Z. H. Zhou, Q. C. Song, K. Y. Chen, G. H. Su, T. Zhou, Z. Zheng, C. H. Lu and X. X. Zhang, *ACS Nano,* 2020, **14**, 7055–7065.

38 Y. He, K. R. Kong, Z. X. Guo, W. F. Fang, Z. Q. Ma, H. H. Pan, R. K. Tang and Z. M. Liu, *Adv. Funct. Mater.,* 2021, **21**, 2101291.

39 L. Y. Yang, J. Cui, L. Zhang, X. R. Xu, X. Chen and D. P. Sun, *Adv. Funct. Mater.,* 2021, **31**, 2101378.

40 L. D. Zhang, S. Chizhik, Y. Z. Wen and P. Naumov, *Adv. Funct. Mater.,* 2016, **26**, 1040–1053.

41 L. D. Zhang, X. X. Qiu, Y. H. Yuan and T. Zhang, *ACS Appl. Mater. Interfaces,* 2017, **9**, 41599–41606.

42 J. K. Mu, G. Wang, H. P. Yan, H. Y. Li, X. M. Wang, E. L. Gao, C. Y. Hou, A. T. C. Pham, L. J. Wu, Q. H. Zhang, Y. G. Li, Z. P. Xu, Y. Guo, E. Reichmanis, H. Z. Wang and M. F. Zhu, *Nat. Commun*., 2018, **9**, 590.

43 R. K. Gogoi and K. Raidongia, *Adv. Mater.,* 2017, **29**, 1701164.

44 H. J. Lin, J. Gong, H. Miao, R. Guterman, H. J. Song, Q. Zhao, J. W. C. Dunlop and J. Y. Yuan, *ACS Appl. Mater. Interfaces,* 2017, **9**, 15148.

45 Y. L. Tan, Z. Y. Chu, Z. H. Jiang, T. J. Hu, G. Y. Li and J. Song, *ACS Nano*, 2017, **11**, 6843−6852.

46 L. D. Zhang, P. Naumov, X. M. Du, Z. G. Hu and J. Wang, *Adv. Mater*., 2017, **29**, 1702231.

Figures and Captions

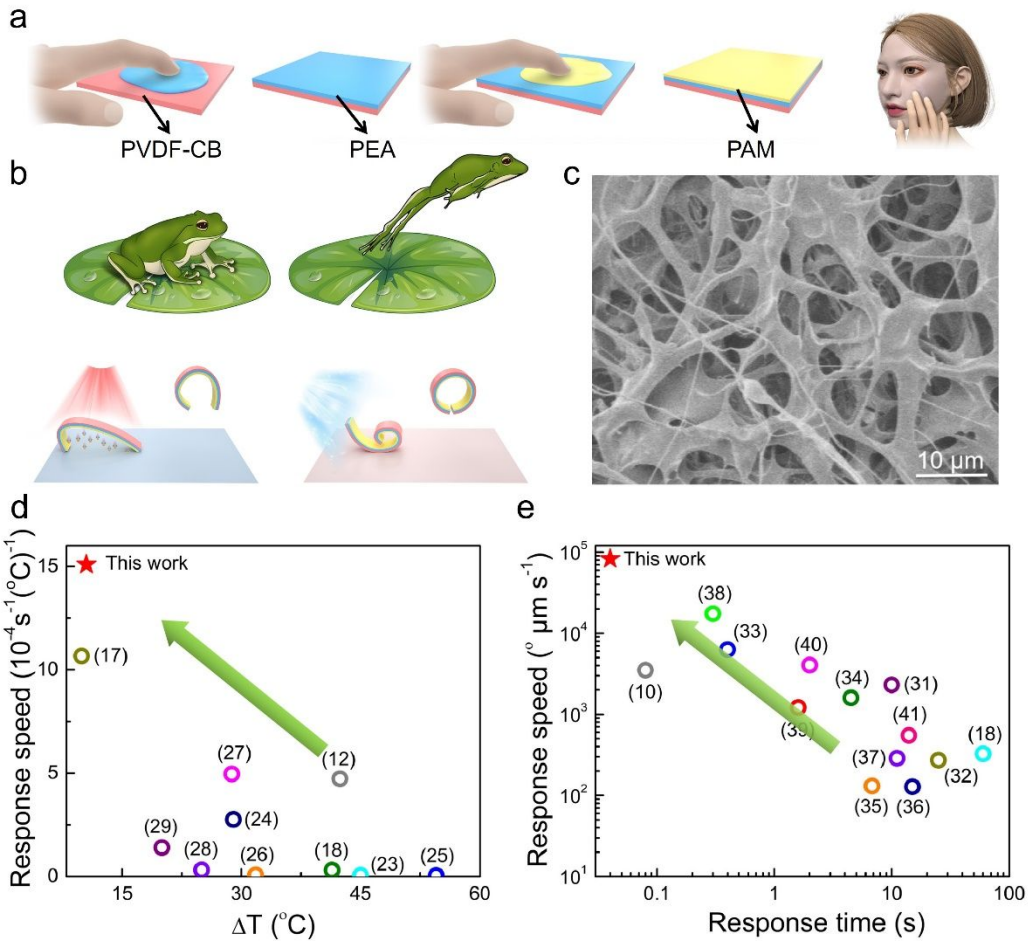

Figure 1. Schematic illustration and characterization of the PVDF-CB/PEA/PAM actuator. (a) Schematic illustration of the PVDF-CB/PEA/PAM jumping actuator inspired by makeup. (b) Schematic illustration of frog-like jumping actuation. (c) SEM image of PAM layer showing the porous structure. (d) Comparison of the bending speed normalized by the thickness and temperature difference of the PVDF-CB/PEA/PAM actuator under NIR irradiation with those of typical actuators in the literature. (e) Comparison of the actuation speed normalized by the thickness and response time of the PVDF-CB/PEA/PAM actuator under moisture stimuli with results from the literature.

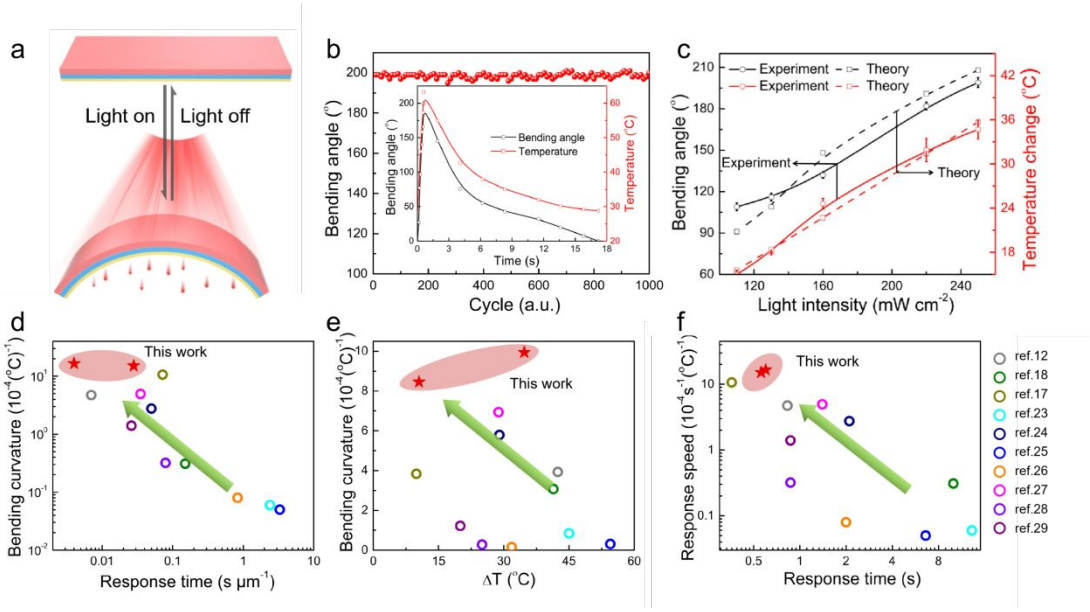

Figure 2. Photothermal actuation of the PVDF-CB/PEA/PAM actuators under NIR light. (a) Schematic illustration of the actuation mechanism in response to NIR light. (b) Repeatable actuation of the PVDF-CB/PEA/PAM actuators exposed to 250 mW cm^{-2} NIR light (the inset is the time dependence of the bending angle and temperature of the actuator). (c) Experimental data and classical Timoshenko beam theoretical analysis of the bending angle and temperature for the PVDF-CB/PEA/PAM actuator as a function of light intensity. (d) Comparison of the bending curvature normalized by the thickness and temperature difference and the thickness-normalized response time of the PVDF-CB/PEA/PAM actuators under NIR irradiation with those of typical photoactuators in the literature. (e) Comparison of the bending curvature normalized by the thickness and temperature difference of the PVDF-CB/PEA/PAM actuators with those of typical photoactuators in the literature. (f) Comparison of the bending speed normalized by the thickness and temperature difference and the response time of the PVDF-CB/PEA/PAM actuators with those of typical photoactuators in the literature. Two types of sizes of PVDF-CB/PEA/PAM actuators were used for (d–f) (15 mm × 2 mm × 20 μm and 15 mm × 2 mm × 150 μm).

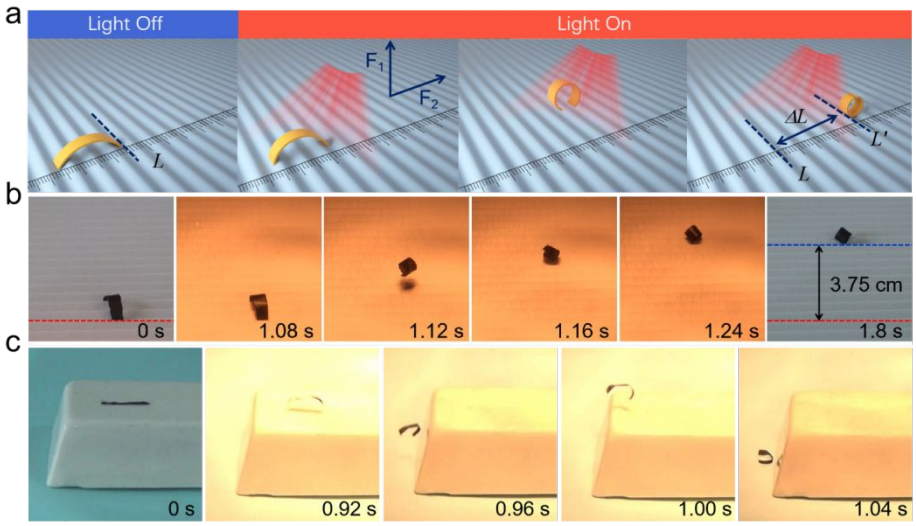

Figure 3. Jumping robot of the PVDF-CB/PEA/PAM actuators under NIR irradiation. (a) Schematic illustration of the jumping robot on a zigzag substrate driven by NIR light. (b) Photographs of the jumping forward robot on the zigzag substrate under NIR illumination. The size of the PVDF-CB/PEA/PAM actuator was 20 mm × 1.5 mm × 20 μm. (c) Photographs of the jumping forward robot on a rough plane under NIR illumination. The size of the PVDF-CB/PEA/PAM actuator was 10 mm × 1.5 mm × 20 μm.

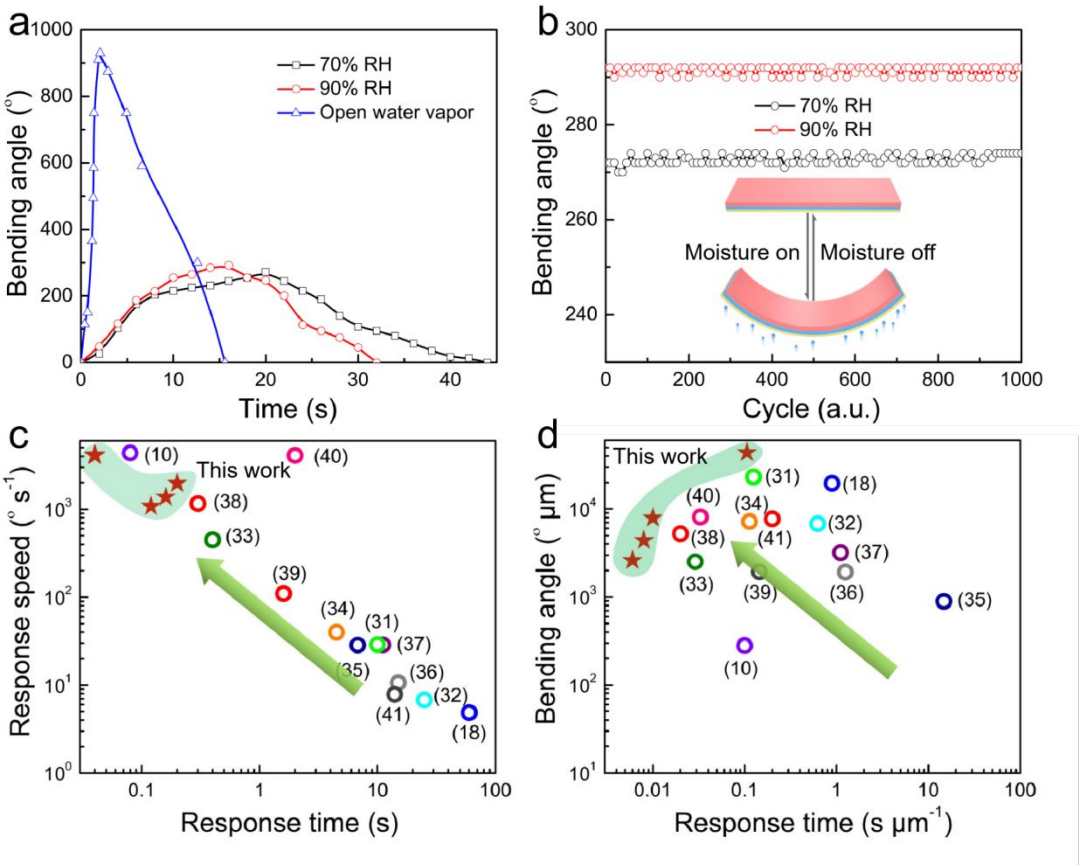

Figure 4. Moisture actuation of the PVDF-CB/PEA/PAM actuators. (a) Time dependence of the bending angle of the 150 μm thick PVDF-CB/PEA/PAM actuator (15 mm × 2 mm) with one end fixed at 70% and 90% RH and the 20 μm thick PVDF-CB/PEA/PAM actuator (11 mm × 1 mm) with both ends free under open water vapour. (b) Bending angle as a function of cycle number for the PVDF-CB/PEA/PAM actuator at RH=70% and 90% (the inset is a schematic illustration of the actuation mechanism in response to moisture). (c) Comparison of the bending speed and response time of the PVDF-CB/PEA/PAM actuator with results from the literature. (d) Comparison of the bending angle and response time normalized by the thickness of the PVDF-CB/PEA/PAM actuator with results from the literature.

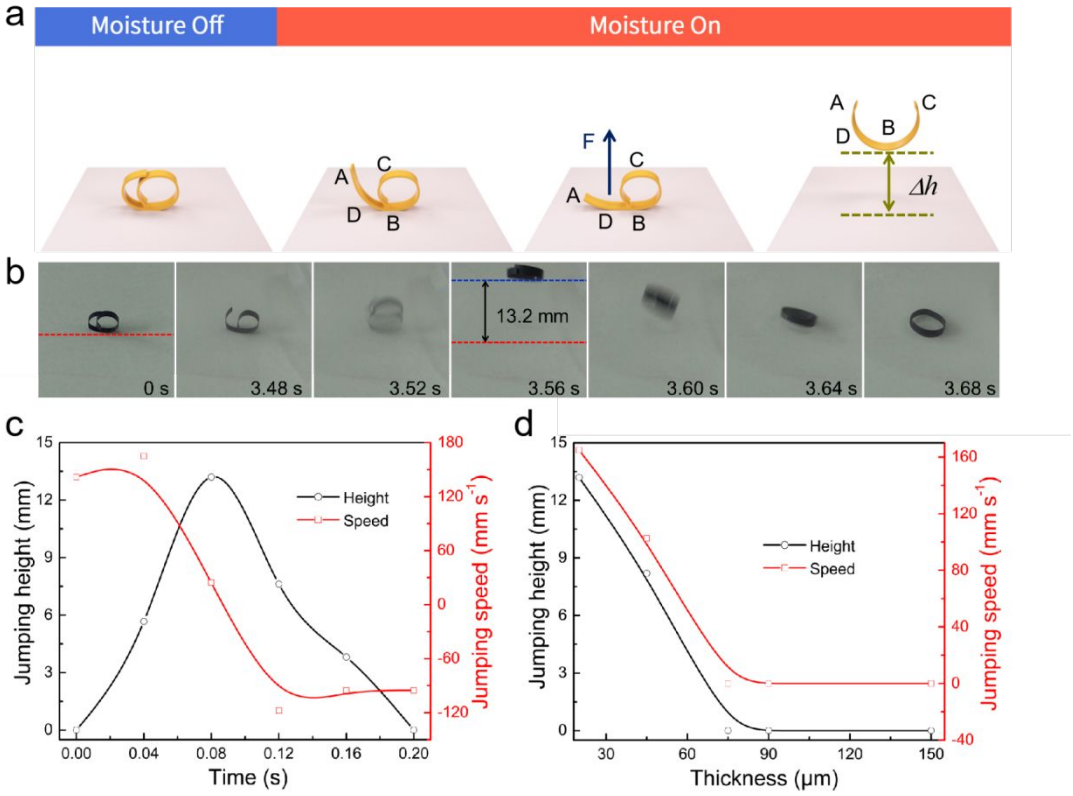

Figure 5. Exposure of the jumping robot based on the PVDF-CB/PEA/PAM actuator to moisture. (a) Schematic illustration and (b) photographs of the jumping process under humidity. The size of the actuator was 20 mm × 1.5 mm × 20 μm. (c) Jumping height and speed as a function of time for the actuator. (d) Jumping height and speed as a function of thickness for the actuator.